Nano Energy 116 (2023) 108796

Contents lists available at ScienceDirect

Nano Energy

journal homepage: www.elsevier.com/locate/nanoen

Opto-iontronic coupling in triboelectric nanogenerator☆

Yaowen Ouyang [a,b], Xiang Li [a,b], Shaoxin Li [a,b], Puguang Peng [a,b], Feiyao Yang [a], Zhong Lin Wang [a,c,*], Di Wei [a,**]

[a] Beijing Institute of Nanoenergy and Nanosystems, Chinese Academy of Sciences, Beijing 101400, China
[b] School of Nanoscience and Engineering, University of Chinese Academy of Sciences, Beijing 100049, China
[c] Georgia Institute of Technology, Atlanta, GA 30332-0245, United States

ARTICLE INFO

Keywords:
Triboelectric nanogenerators
Opto-iontronic rectification
Remote charging

ABSTRACT

Triboelectric nanogenerator (TENG) has received tremendous attentions for its ability to convert mechanical energy into electrical energy. However, the induced current generated by TENG is an alternating-current (AC) signal and cannot directly satisfy most electronic devices that require direct-current (DC) supply. As a result, there has been a great number of interests in developing DC-TENG. Here, we have successfully developed an alternative to rectify TENG for DC output by coupling the electronic displacement current of TENG with ionic current, which could be further replenished by photocurrent. For the first time, an opto-iontronic current coupling in TENG was achieved under UV irradiation. A photogenerated electric field is triggered to remotely manipulate ion migration to complement the dissipation of ion concentration gradient. This permits the ionic current to be continually generated to rectify the electronic displacement current from the TENG in the opposite direction, while allowing coupling of both ionic and electronic current in the same direction. The opto-iontronic DC-TENG could be fabricated into one integrated flexible and thin device and the ionic charge could be remotely replenished by UV light. This study introduces a rectification paradigm for TENG and provides an effective method for in-situ AC-DC conversion, which could be potentially applied in wearable devices, bioelectronics, and self-powered intelligent sensors.

1. Introduction

With the development of internet of things supported by numerous sensor networks in the era of Big Data [1,2], TENG has attracted tremendous attentions as an green energy harvesting technology, due to its ability to convert mechanical energy to electrical energy, in addition to its low cost, wide choice of materials, and simplicity of fabrication [3–6]. However, conventional TENGs are limited by the AC output signal and cannot directly satisfy electronic equipment with DC demands [7,8]. The AC signals can be generally converted to DC signals by an external rectifier bridge or a mechanical brush in TENG, which would inevitably cause complexity in the design of the integrated devices and limit its applications in many areas such as flexible or wearable electronics [9–13]. DC-TENGs have attracted broad interests in a variety of perspective applications [14,15]. The mechanism of conventional DC-TENGs could be broadly classified into phase coupling [16,17], dielectric breakdown [18], and semiconductor-based tribovoltaic effects [19–22], each of which has pros and cons with intrinsic limitations. For example, phase coupling requires a specific structural design, usually complex and large; dielectric breakdown requires ultra-high breakdown voltages; semiconductor-based nanogenerators frequently require the employment of sliding friction modes, which unavoidably accelerates material deterioration with limited material selection [23]. Types of DC-TENG with simple fabrication, low friction on materials and a broad selection of materials for perspective applications are desperately needed for its application in the ubiquitous internet of things.

In electronics, the charge carriers are electrons and holes, but the information in biological systems is transmitted by a large variety of ions, including Na^+, K^+, Cl^-, Ca^{2+} and so on [24]. Unlike electrons, the ionic charge carrier is well protected from electrical or magnetic noises.

☆ Prof Zhong Lin Wang, an author on this paper, is the Editor-in-Chief of Nano Energy, but he had no involvement in the peer review process used to assess this work submitted to Nano Energy. This paper was assessed, and the corresponding peer review managed by Professor Chenguo Hu, also an Associate Editor in Nano Energy.

* Corresponding author at: Beijing Institute of Nanoenergy and Nanosystems, Chinese Academy of Sciences, Beijing 101400, China.
** Corresponding author.
E-mail addresses: zhong.wang@mse.gatech.edu (Z.L. Wang), weidi@binn.cas.cn (D. Wei).

https://doi.org/10.1016/j.nanoen.2023.108796
Received 14 June 2023; Received in revised form 15 August 2023; Accepted 16 August 2023
Available online 18 August 2023

Moreover, the electron is singular as a carrier, in contrast, ions have different valences, sizes, polarizabilities, and other properties that can be utilized to create more efficient and diversified iontronics [25], which is promising to create biocompatible human-machine interfaces [26–28]. Iontronics, as an emerging interdisciplinary concept, focus on the science and technology of electronic-ionic coupling properties, covering electrochemistry, solid-state physics, electrical engineering, and biosciences [29–31]. Iontronics also allow us to achieve new functions and properties that are extremely difficult or even impossible in conventional electronic devices [32–34]. Based on the nanoconfined effect of the 2D nanofluidic material, asymmetric unidirectional transport of K^+ in the nanofluidic channels can be achieved, resulting in ion permeation current based on salinity gradient [35–37]. The unidirectional selective conduction of ions within 2D nanofluidic channels can be used to mimic the transmembrane transport of ions by cell membranes as in the activity of life. More interestingly, the photogenerated electric field by light irradiation on 2D nanofluidic materials enables active transport of ions across a reverse concentration gradient, which satisfies the basic requirements for artificial photosynthesis [38,39].

Here, an alternative to rectify TENG for DC output is developed by integrating an opto-iontronic unit into a TENG in contact-separation mode, rectifying electronic currents through ionic currents. The opto-iontronic device is made of 2D nanofluidic material of graphene oxide (GO) and reduced graphene oxide (rGO) that was obtained by mild reduction of GO by KOH. Under specific humidity conditions, the generation of ionic current is controlled synchronously by the contact and separation movement patterns of the TENG. The ionic current generated from salinity gradient will decrease with the depletion of the ion concentration. For a continuous DC output, the electric field generated by ultraviolet (UV) irradiation on GO or rGO was found to be able to regulate the migration of ions, suggesting that by irradiation we could achieve a remote ionic charge replenishment. Furthermore, the remote supplementation of the ionic charge by UV light also means that we have realized an approach to controllable AC-DC signal conversion approach on a single TENG, simplifying the integrated system design. This work also presents a strategy for the detection of UV and other radiation by the DC-TENGs through the conversion of signal modes. It opens scenarios in many perspective applications through the electronic-ionic coupling interface.

2. Results and discussion

Traditional TENG could only generate AC signals, difficult to be directly applied to electronics that required DC supply. To the best of our knowledge, there are few reports on the TENG rectified by ionic current.

Photograph of the iontronic DC-TENG was shown in Fig. 1a, in which GO film, rGO film and Kapton film all had an effective area of 1 cm^2, respectively. The electrodes of opto-iontronic DC-TENG were made of transparent ITO for UV light to pass through. ITO electrode was flexible and thin, so the GO or rGO film prepared on its surface also had a certain bending ability, and the bending radius was about 0.35 cm (Fig. S1). The rGO-coated ITO electrode and the GO-coated ITO electrode were referred to as electrode-I and electrode-II, respectively. By simply coating the GO and rGO inks on different sides of the electrode, opto-iontronic device could be easily integrated with TENG. rGO (containing K^+) and GO films were used to provide ionic current ($\boldsymbol{I_i}$), and K^+ was observed to migrate from rGO through 2D nanofluidic channels of GO when solid-state GO/rGO junction was formed at ambient humidity environment in our previous work [40,41]. The thickness of GO and rGO membranes measured by 3D surface profilers was around 4–6 μm (Fig. S2). The thickness of the GO and rGO film was increased from 6 μm to 12 μm and 18 μm respectively to test the effect of film thickness on device performance (Fig. S3). With the increase in the film thickness, the $\boldsymbol{V}_{oc}$ changed little, keeping around 1 V. In contrast, the $\boldsymbol{I}_{sc}$ decreased significantly from 0.07 μA to 0.02 μA with the increase in film thickness from 6 μm to 12 μm. This might be the increase in GO film thickness made the resistance larger, resulting in the greatly reduced current. When the thickness of the film was further increased to 18 μm, the decrease in $\boldsymbol{I}_{sc}$ was not significant. It might be ascribed to the limited penetration of humidity on the film. Kapton film attached on the electrode-II was chosen as the dielectric material layer to better match the impedance between the ionic current source and TENG (Fig. S4). The coupling relationship between the electronic current and the opto-iontronic modulation of the ions by UV irradiation was illustrated in Fig. 1b. TENG could only generate AC electronic current $\boldsymbol{I_e}$ [Fig. 1b (i)]. Based on the TENG structure, the unidirectional ionic current $\boldsymbol{I_i}$ provided by GO/rGO junction was introduced to realize the rectification by counteracting $\boldsymbol{I_e}$ generated by TENG in the opposite direction [Fig. 1b (ii)]. Hence, the electronic-ionic coupling presented a DC current in the external circuit. However, the gradient balance of K^+ would cause $\boldsymbol{I_i}$ to decay to a certain threshold (defined as $\boldsymbol{I'_i}$), which could not achieve the rectification effect on $\boldsymbol{I_e}$. At this point, the built-in electric field ($\boldsymbol{E_{bulit}}$) could be generated by irradiating rGO with UV light source to construct a new ion concentration gradient and enhance the ionic current. The current generated by the UV was defined as $\boldsymbol{I_{bulit}}$, and the opto-iontronic strategy could achieve the sustainable rectification of the ionic current to the electronic current [Fig. 1b (iii)]. Areal and volumetric peak power density of the DC-TENG was respectively obtained as 0.17 mW/m^2 and 1.55 mW/m^3 at RH= 60% (Fig. 1c), and maximum transferred charge density was calculated to be about 69 $\mu C/m^2$. When RH≤ 40%, the integrated device generated an AC signal, which indicated that the electronic current generated by TENG dominated (Fig. 1d and e) at lower humidity level. This might be due to that low humidity was not sufficient enough to trigger efficient K^+ migration and therefore could not generate matched ionic currents for rectification. Under RH= 60%, K^+ could transport efficiently within the 2D nanofluidic channels of GO, and the generated ionic current could counteract the electronic displacement current of TENG in the opposite direction, thus exhibiting DC signal (Fig. 1f). It is noteworthy that the concentration gradient would keep for a very long time because the rGO containing large amount of K^+ was in the solid form and kept almost at the saturated state. K^+ embedded inside the rGO layer would only be driven through the 2D nanofluidic channels of GO when electrode-I and electrode-II were in contact under humidity. Thus, the ionic rectification still remained after 7000 cycles under RH= 60% (Fig. S5). However, when the balance of ion concentration was reached, it might eventually exhibit an AC signal. Remote supplementation of ionic charge by UV irradiation in this paper was shown as an effective way. The UV irradiation might draw more K^+ cations to the rGO/GO interface to refill the concentration gradient. Supplementing charge itself had been tried in TENG by modification of triboelectric polymer materials to enhance charge density, or by control of environmental influences (temperature, vacuum, humidity, etc.), or by ultra-thin dielectric layers and liquid lubrication [42–47]. None of them could be realized in-situ or controlled remotely. As shown in Fig. 1g, by UV irradiation on the rGO, the peak current of the DC-TENG reached a maximum value of about 8 μA from about 0.4 μA. More importantly, the conversion of AC signal to DC signal was directly observed during the experiment, which demonstrated the feasibility of coupling ionic current with electronic current in the DC-TENG.

Such effect of turning AC into DC before and after UV irradiation could also be used in UV light detecting sensors. For example, the switching of the signal mode could be used to perceive the light irradiation including UV light in the environment, so as to realize the early warning protection function. To realize the transformation of AC-DC signal of TENG, it was generally necessary to couple an external rectifier bridge and design a special power management system [48], or by combining an AC-TENG with a DC-TENG [49]. Here, the conversion of two different signals could be achieved by remotely replenishing the ionic charge with UV irradiation on a single TENG. There was also a significant change in the amount of transferred charge before and after irradiation, indicating that UV irradiation produced an effective charge

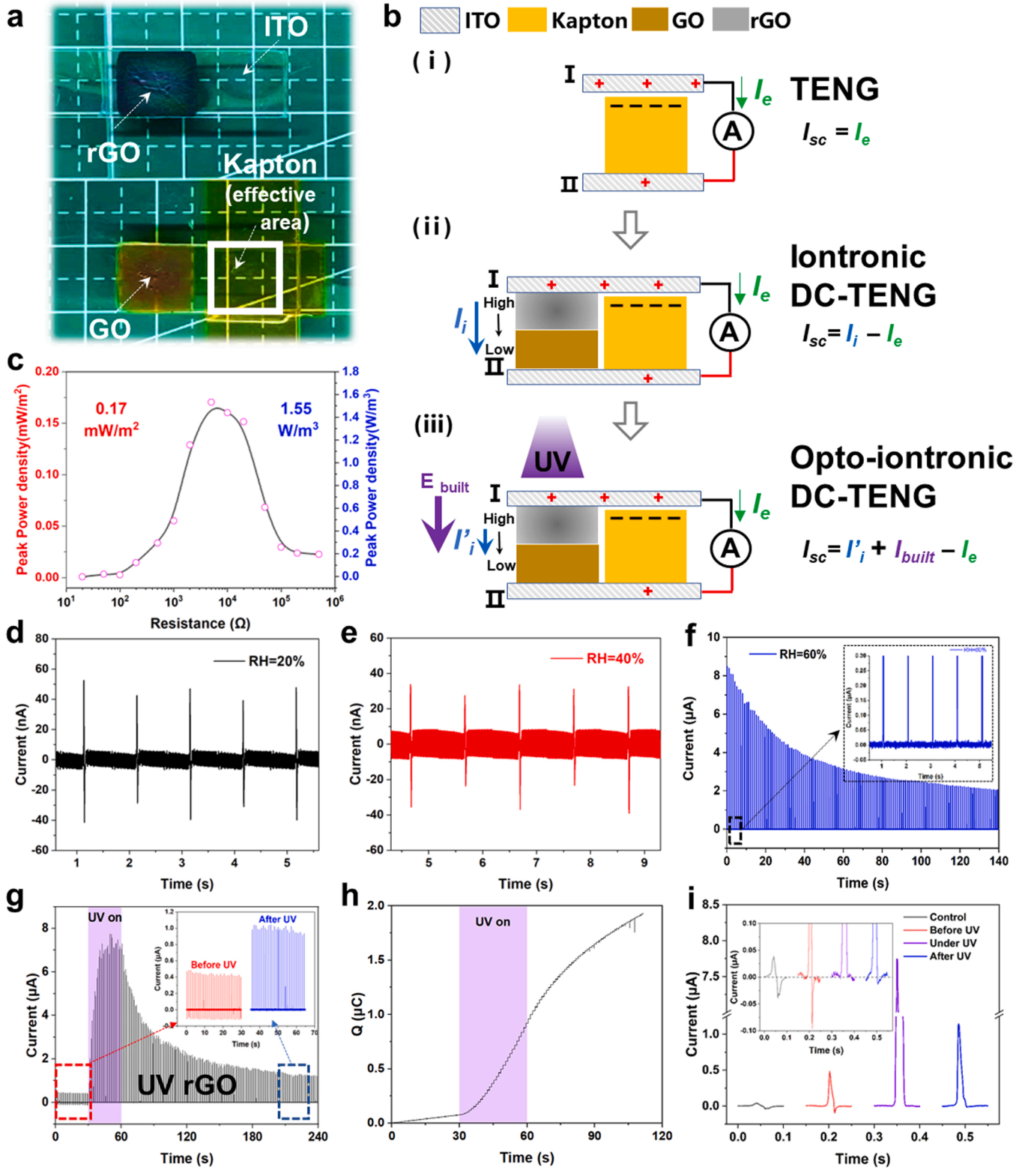

Fig. 1. DC-TENG structure and its performance. (a) Photograph of the iontronic DC-TENG. (b) Schematic of the TENG, iontronic DC-TENG and opto-iontronic DC-TENG and their mechanisms when electrode-I is approaching electrode-II. (c) Peak current power density as a function of load resistance. Current signal of iontronic DC-TENG at different humidity (d) RH= 20%, (e) RH= 40% and (f) RH= 60%, respectively. Photo-rectification effect of opto-iontronic DC-TENG, (g) Current and (h) transferred charge, all experiments were performed using a UV lamp with a wavelength of 365 nm and an irradiation power of 350 mW/cm^2 for 30 s (i) Comparison of current wave patterns of TENG, iontronic DC-TENG before UV irradiation, opto-iontronic DC-TENG under UV and after UV for a period of time, respectively.

replenishment (Fig. 1h). Similar effect could also be observed by UV irradiation on the GO (Fig. S6). However, in the charge/discharge cycles by UV irradiation experiments, the maximum photo-charging voltage generated from the GO side decreased with increasing UV irradiation times, while the one from rGO did not decrease (Fig. S7). Therefore, UV irradiation on the rGO side was considered to be a preferable option. Such different phenomenon between GO and rGO might be related to the complex photochemical reactions of GO being reduced to defective carbon [50,51], which is possibly attributed to the elimination of C═O [52,53]. The change in the current wave pattern after UV irradiation was showed in Fig. 1i, and the displacement electronic current of TENG under the same environmental condition without UV irradiation was shown as control. The positive current might be mainly due to the ionic current peak, and the negative current might be caused by the electronic current. When the salinity gradient was reaching balance, the ionic current was weakened to the point that the reverse electronic current generated by TENG could not be fully offset, so the overall current waveform started to be presented in an AC form (Before UV). Once the ionic charge was supplemented by UV irradiation (Under UV), the electronic current peak disappeared, and the ionic current peak width was broadened, indicating the ionic rectification of the electronic current. When the UV was off for a while (After UV), the ionic current was still dominated to rectify the electronic current to generate the DC output. This phenomenon also proved that UV could successfully supplemented the ionic charge.

To further study the rectification effect of ionic current on electronic current, TENG, the iontronic unit and the integrated DC-TENG were prepared, and their performances were compared. Fig. 2a-d illustrated the structure and output performance of the TENG, and the output capability decreased with increasing humidity. This fact could be ascribed to that hydrophilic Kapton film surface tended to retain water layer, which might shield the polymer surface to prevent effective charge transfer between the two contacting surfaces, leading to the decreased output performance of the TENG [54–56]. As shown in Fig. 2e-h, the iontronic unit was a DC ionic current source, and it generated greater current output with increased humidity. When the iontronic unit was combined with the TENG as shown in Fig. 2i, there was a weak AC signal at low humidity conditions, and DC signal would appear when the RH reached 60% (Fig. 2j-k). It was especially worth noting that when the RH reached 40%, the iontronic unit exhibited a DC signal, but the integrated TENG still maintained an AC signal. This phenomenon indicated that electronic current produced by TENG still dominated and it was difficult for the generated ionic current to rectify it, resulting in the coupled output signal as a weak AC signal. Once the RH was raised to 60%, the ionic current dominated and a unidirectional current was achieved. Interestingly, TENG was a device with high voltage and low current characteristics, while iontronic device had low voltage and high current characteristics. The voltage of TENG reached about 2 V at RH= 60%, while iontronic unit itself was only about 0.35 V. When the two were coupled, the voltage value was around 1 V, and the peak pattern showed a partial superposition of the two. The TENG rectified by the ionic current offers synergized benefits of decent current and voltage supply. Interestingly, $\mathbf{I_{sc}}$ in Fig. 2j was larger than that in Fig. 2f, which indicated that the electron displacement current might promote the ionic current. Furthermore, the effect of frequency variation was studied for a maximum DC frequency of 1 Hz (Fig. S8). This was very compatible with the frequency of human motion. With higher frequencies (>1 Hz), the rectification effect diminished, which could be attributed to the fact that the ions migrated much slower than the electrons.

The use of the iontronic unit to counteract the AC electronic current signal in one direction of the TENG was successfully realized by the

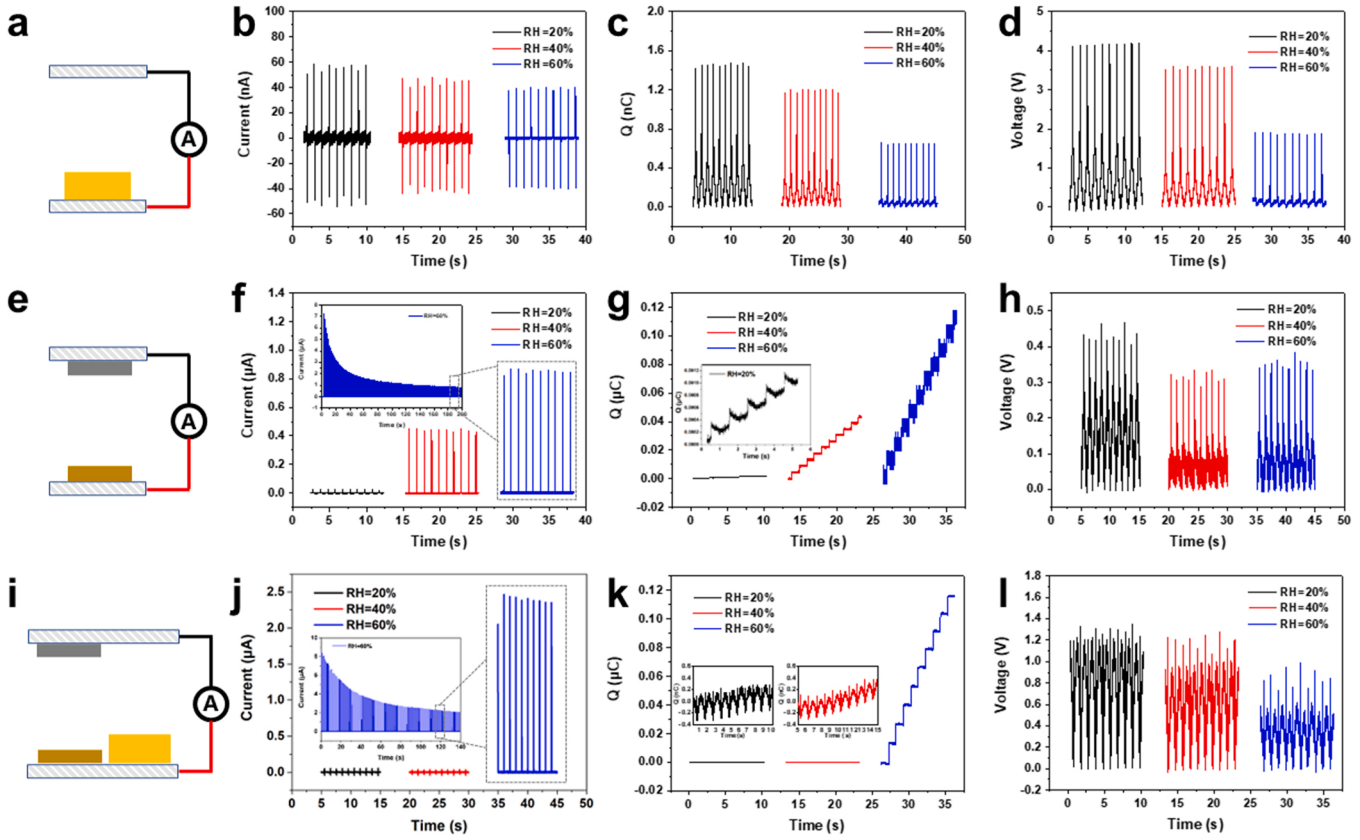

Fig. 2. Performance comparison. (a) the structure of TENG, (b), (c) and (d) refer to the current (***I***), transferred charge (***Q***) and voltage (***V***) of TENG under three different RHs of 20%, 40%, 60% respectively. (e) the iontronic unit as the ionic current source, and (f), (g), (h) refer to its *I*, *Q*, *V* under different RH. (i) the iontronic DC-TENG, and (j), (k), (l) refer to its ***I***, ***Q***, ***V*** under different RH.

integrated device, meanwhile, the current in the other direction would be reinforced via the coupling of both electronic and ionic current. To further investigate the rectification mechanism, the position of the dielectric layer (Kapton) located on electrode was altered. The Kapton film attached on the electrode-I was defined as **Structure-1**, and that attached on electrode-II was defined as **Structure-2,** as shown in Fig. 3a and b respectively. Interestingly, **Structure-1** generated only AC signal, in contrast, a significant rectification effect could be observed in **Structure-2**. The position of Kapton played an important role in the influence of ionic current, which might be due to the induced potential generated by the two electrodes during contact electrification (CE). It might have a certain influence on the migration of ions.

As Kapton film was generally more electronegative, the surface of it tended to be negatively charged when in contact with ITO. In **Structure-1**, when the Kapton film fixed on electrode-I gradually approached electrode-II with a negatively charged surface [Fig. 3a(ii)], electrons flew from electrode-II to electrode-I, forming a negative electronic current (I_{e1}) due to the electrostatic induction effect. The electrons migration rate was much quicker than the ions and the increase in the positive charge on electrode-II might inhibit the migration rate of K^+ from rGO to GO [Fig. 3a(v)]. Therefore, negative I_{e1} appeared at first and then small ionic current (I_{i1}) that need to overcome the built-in electric field occurred during the contacting process. When Kapton was fully contacted with ITO [Fig. 3a(iii)], the peak value of I_{sc} was only ca. 0.35 μA shown in [Fig. 3a(vi)], which might also be attributed to the inhibition of K^+ migration with the increase in positive charge on electrode-II. In the process of separating [Fig. 3a(iv)], the electrons migrated from electrode-I back to electrode-II forming a positive electronic current (I'_{e1}) and coupled with I_{i1}. In **Structure-2**, when electrode-I was approaching to electrode-II fixed with Kapton film [Fig. 3b(ii)], electrons flew from electrode-I to electrode-II due to electrostatic induction effect, forming a positive electronic current (I_{e2}). However, at this time, the increase in the positive charge on electrode-I promoted the migration of K^+ from rGO to GO. K^+ was facilitated to migrate from rGO to GO, and positive I_{e2} was coupled with positive ionic current (I_{i2}). When fully contacted [Fig. 3b(iii)], it reached a current peak around 8μA [Fig. 3b(vi)] due to the promotion of K^+ migration by the increase in positive charge on electrode-I [Fig. 3b(v)]. In the process of separating [Fig. 3b(iv)], electrons flew from electrode-II back to electrode-I to form a negative I'_{e2}, which was rectified by the positive I_{i2} to be finally presented as a DC signal.

The relationship between ionic and photoelectric currents was further explored. It was reported that the migration of ions might be regulated by the built-in electric field generated by the absorption of UV of GO-like materials. The direction of the built-in electric field was the same as the pointing direction of the light source [57]. When a finite thickness material was fully exposed to light, the carrier concentration on the surface was higher than that on the inside. At this time, the difference of carrier concentration in the depth direction drove the diffusion of electrons and holes from higher to lower levels, and the difference in the diffusion rate of electrons and holes formed the built-in electric field, which enabled the migrating of ions [57]. To verify the mechanism, a series of experiments were designed by alternating direction of the built-in electric field. Firstly, the physical and chemical

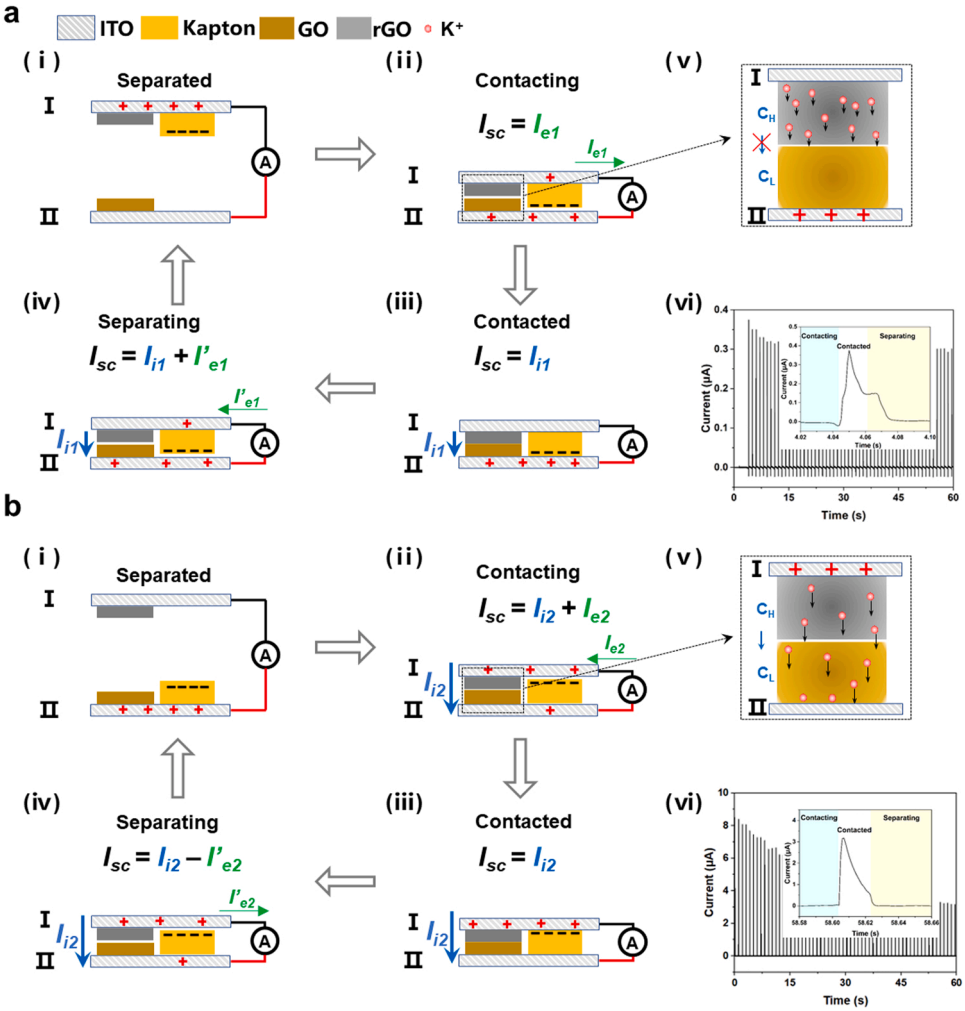

Fig. 3. Diagram of working principle of iontronic TENG with (a) and (b) two different structures and corresponding mechanisms under RH of 60%.

properties of GO and rGO and the effect of UV irradiation on them were characterized. The XRD results showed that the interplanar spacing of GO in this paper was slightly larger than that of rGO. It might be ascribed to that the rGO particles might accumulate more compactly during the film formation process (Fig. S9). No obvious changes were observed on the surface of GO and rGO after different UV treatment times in the SEM, indicating that the irradiation power (365 nm, 350 mW/cm^2) and irradiation time (30 s each time) might not cause significant chemical changes in the material (Fig. S10). The main difference between the rGO and GO in the FTIR was reflected in the disappearance of the C═O peak at 1750 cm^{-1} (Fig. S11), which indicated that many carboxylic groups might be washed off by KOH [58]. The GO and rGO solutions under different UV irradiation time were also characterized by UV-Vis spectroscopy (Fig. S12). A strong absorption peak at 229 nm and a shoulder peak at 290–340 nm were detected. The former peak was related to π-π * transitions of aromatic C═C bonds, and the latter peak was originated from the nπ* - type electron transitions in carbonyl groups [59]. With the increase in irradiation time, the peak at 229 nm basically did not change significantly, while the peak at 290–340 nm shifted upward, which indicated that both GO and rGO, especially rGO might be further reduced by UV to some extent [60]. The temperature change under UV irradiation was tested using a thermal imager (Fig. S13). The temperature under 30 s irradiation on GO was only 32 ℃, and it basically remained at 40 ℃ after 10 min of continuous UV exposure. Although some reports indicated that high-temperature reduced GO nanosheets were found to be an effective thermoelectric conversion material, such experiments were conducted using temperatures up to about 3000 K to reduce GO [61]. In contrast, the temperature change in our experiments was far below the reported temperature, and the thermal effects on the ions migration in our experiments might have negligible influence [62].

The photoelectric effect of irradiated GO or rGO was tested under different humidity to verify the direction of the photo-generated built-in field. As the humidity increased, the short-circuit current ($\boldsymbol{I}_{sc}$) continued to rise. Interestingly, the current direction was opposite for GO and rGO film under UV-irradiation (Fig. S14). For GO film, the photoelectric current might be due to the reduction, and it was in the pA level (max. ca. 140 pA) with positive current direction under RH 60%. As reported that the photogenerated built-in electric field was in the same direction as the pointing direction of the light source [57]. In case of rGO which contained large amount of K^+, the photogenerated electric field promoted ion migration and ionic current dominated, generating current in nA level (max. ca. 2.5 nA much higher than that of GO film) with the negative current direction under RH 60%. Similarly, higher charge was transferred for rGO than GO (Fig. S15). To verify the formation of the built-in electric field and the effect of water, a non-aqueous solvent of dimethyl sulfoxide (DMSO) was chosen as solvent. Different concentrations of ionic liquid of bistrifluoromethanesulfonimide lithium (LiTFSI) dissolved in DMSO were coated on the ITO surface of electrode-I and then only GO or rGO was sandwiched between the LiTFSI-DMSO coated electrode-I and electrode-II (Figs. S16 and S17). The experiment results showed that a pronounced current was observed when using DMSO, and this might be due to the infiltration of DMSO into the 2D nanofluidic channels of GO or rGO resulting in a further decrease in the ionic resistance. So, the current in the opto-iontronic DC-TENG under UV irradiation might not come from catalysis of water, and the formation of the built-in electric field was not affected by the type of solvent. When UV irradiation was applied from two different directions, the direction of the generated $\boldsymbol{I}_{sc}$ from GO or rGO sandwiched between ITO electrodes was completely different. In case of GO film, when the UV lamp irradiated either electrode-I or electrode-II, the current direction both showed positive, and did not change when altering the light source direction. When the light source was pointing to electrode-II (Fig. S16a), there was no significant difference in the current value between pure DMSO and 0.1 M LiTFSI in DMSO (both ca. 15 nA), which might be attributed to the built-in electric field inhibiting the salinity-gradient-driven migration of Li^+ from LiTFSI on electrode-I. As the concentration of LiTFSI solution increased to 1 M, the current increased to 25 nA, which might be due to the amplified ion migration under increased salinity gradient. However, once the light source was pointing to electrode-I (Fig. S16b), the current values from pure DMSO (9 nA) and 0.1 M LiTFSI in DMSO (20 nA) were quite different. This might be because the built-in electric field accelerated the diffusion of Li^+ from electrode-I to the electrode-II, forming a positive ionic current, which was stronger than the electronic current, hence, the overall current direction was still positive. As the concentration of LiTFSI was increased to 1 M, the detected ionic current did not change much (ca. 22 nA). However, rGO showed the changes in current direction when altering the irradiation direction, which might be attributed to the fact that rGO contained a large amount of K^+. When the light direction was pointing to electrode-II (Fig. S16c), the built-in electric field accelerated the diffusion of K^+ to the electrode-I. The enhanced diffusion of K^+ inhibited the migration of Li^+ from electrode-I to electrode-II. So, the dominant current direction of ionic current was negative, which was further supported by the fact that the magnitude of the negative current decreased with increasing the concentration of Li^+ (from 40 nA to 12 nA and to 4.5 nA, in the order of 0 M LiTFSI in DMSO, 0.1 M LiTFSI in DMSO and 1 M LiTFSI in DMSO respectively). When the light direction was pointing to electrode-I (Fig. S16d), the built-in electric field enhanced the diffusion of Li^+ to electrode-II. The built-in electric field together with the salinity gradient of K^+ strengthened both the migration of Li^+ and K^+ to the electrode-II, so the dominant current direction of ionic current was positive and larger (ca. 30 nA). It was worth noting that sharp peaks generated instantaneously under UV irradiation were prevalent in the experimental groups containing Li^+ relative to the control group of pure DMSO solvents, which might be attributed to the faster migration rate of Li^+ with smaller size. To verify once again the orientation of the built-in electric field, both GO and rGO were assembled into a junction and the current and charge under irradiated GO and rGO respectively were tested directly with a 6514 electrostatic meter (Figs. S18 and S19). In the ITO/rGO/GO/ITO device, the current magnitude from irradiated rGO (around 150 nA) was much larger than that of irradiated GO (around 45 nA) at RH= 60%, which again supported the assumption that the direction of the photogenerated built-in electric field coincided with the direction of irradiation and the increase in current was due to the synergic effect from salinity gradient from K^+ in rGO.

After investigating the orientation of the photogenerated built-in electric field, the relationship between the photoelectric current and the ionic current was further characterized by electrochemical methods on the opto-iontronic device. The photograph of the opto-iontronic unit was showed in Fig. 4a. The $\boldsymbol{V}_{oc}$ and $\boldsymbol{I}_{sc}$ could be obtained by the intercepts on the current and voltage axes by applying a sweeping voltage from 1.5 V to 0. $\boldsymbol{V}_{oc}$ stayed at around 1 V and did not change significantly with increasing humidity, but the $\boldsymbol{I}_{sc}$ increased from 0.03 μA to 0.11 μA (Fig. 4b). This phenomenon could also be attributed to that more efficient unipolar ion transport of K^+ within 2D nanofluidic channels of GO as the RH was increased [41,63]. The Nyquist plot of electrochemical impedance spectroscopy (EIS) under different humidity was shown in Fig. 4c, and it also showed significant decrease in charge transfer resistance (R_{ct}) from 1.96 MΩ to 30.61 KΩ (from RH=20% to RH=60%) indicating more efficient ionic transport at higher RH (Fig. S20). Fig. 4d showed that the opto-iontronic device had a longer discharge time (ca. 420 s) under RH= 60% than RH= 40% (ca. 23 s) (Fig. S21) when discharged at a constant current of 10 nA. This could also be attributed to that more ions migrated with the increasing of humidity. Fig. 4e showed that the significant ion modulation effect upon UV irradiation of rGO, and the effect of irradiating GO was shown in Fig. S22. The increase in voltage upon UV irradiation of rGO (around 0.2 V in Fig. 4e) might be attributed to the superposition of the $\boldsymbol{E}_{built}$ and $\boldsymbol{E}_{i}$. The UV irradiation effect on both GO and rGO were studied, and the I-V curves showed that the irradiated rGO generated a rectification effect under RH= 60% (Fig. 4f). The results in low humidity conditions

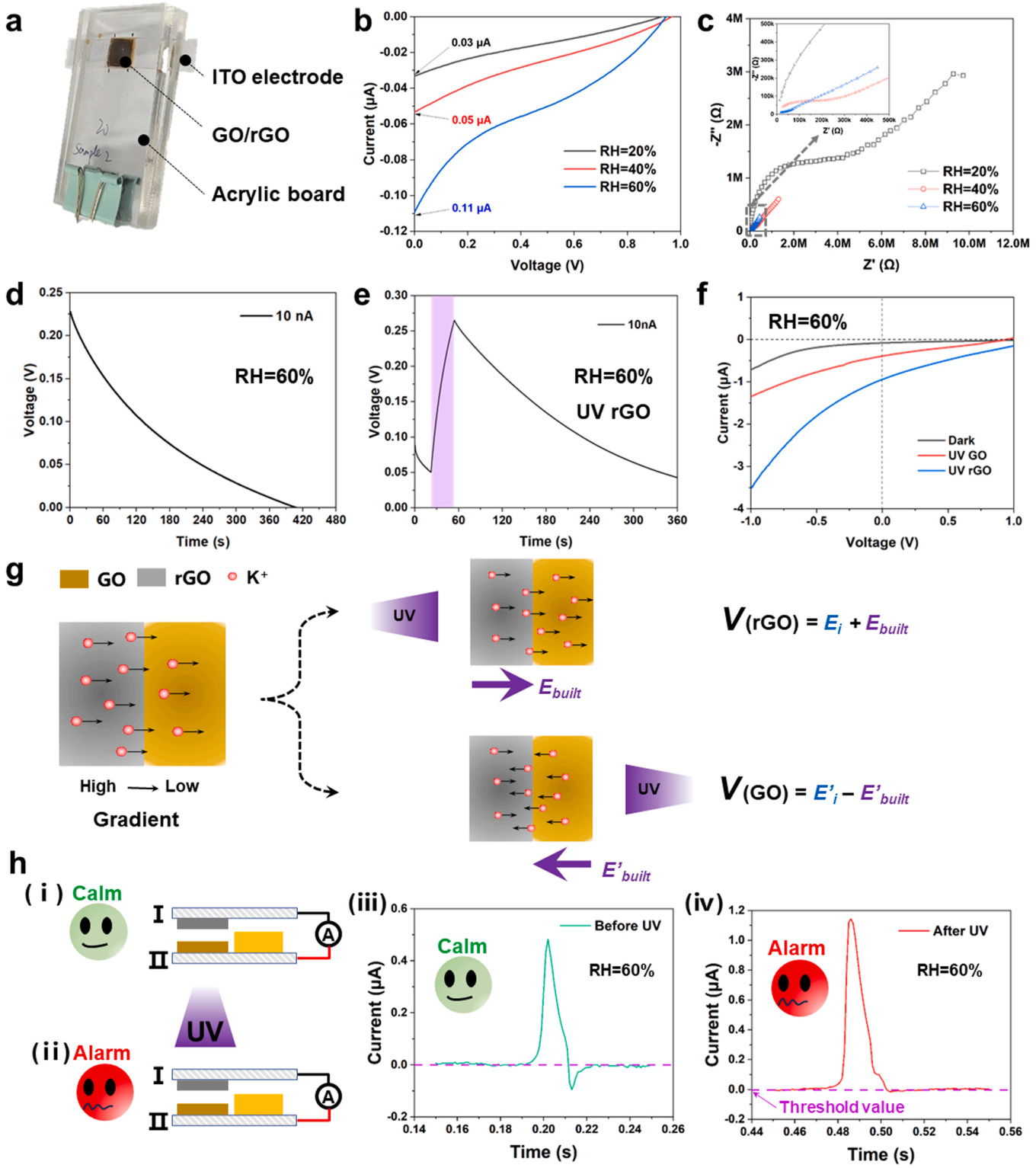

Fig. 4. Electrochemical properties of Opto-iontronic unit, and the application schematic of iontronic DC-TENG as a UV photodetector. (a) Photograph of the opto-iontronic device. (b) *I-V* characteristic and (c) The Nyquist plot of electrochemical impedance spectroscopy (EIS) under different humidity. (d) The 10 nA constant current discharge curves at RH= 60%. (e) UV light charge-discharge curves at RH= 60%, with irradiation time of 30 s and irradiation power fixed at 350 mW/cm^2. (f) *I-V* curves of UV irradiated GO or rGO, respectively. (g) Schematic diagram of the photo modulation mechanism. (h) The application diagram of iontronic DC-TENG as a UV photodetector.

were shown in the Fig. S23. The mechanism of light-regulated ion migration was shown in Fig. 4g. When the GO side was irradiated, the direction of the built-in electric field was against the salinity gradient of K^+. In contrast, the direction of the built-in electric field when the rGO side was irradiated coincided with the salinity gradient of K^+. The former inhibited the diffusion of K^+ from the rGO into the GO, while the latter facilitated K^+ migration. Therefore, the current from the irradiated GO side was much smaller than that from the rGO side. We also

tested the EIS when irradiating GO and rGO separately, and the resistance when irradiated rGO was smaller than GO (Fig. S24). This might be attributed to the stronger absorption of UV by rGO, so more photogenerated carriers made the resistance smaller [64]. The switching of the AC into DC could be used to perceive the light irradiation including UV light in the environment, so as to realize the early warning protection function. After the ion concentration balance, an AC signal would be presented, which was set to the ' Calm ' state [Fig. 4h(iii)]. When the GO/rGO junction irradiated by UV, the current signal transfer from AC signal to DC signal. At this time, it becomes an ' Alarm ' state and warns against UV irradiation [Fig. 4h(iv)].

3. Conclusions

In this work, an alternative to rectify TENG for DC output was successfully prepared by coupling the opto-iontronic unit with TENG. For the first time coupling of ionic current with electronic current for DC output was realized, and its rectification mechanism was proposed. In opto-iontronic DC-TENG, the ionic current could synergize the electronic current and the photoelectric current in the integrated flexible and thin device. The relationship between photoelectric current and ionic current had been further investigated. The influence of water on the opto-iontronic DC-TENG was studied, and the direction of the built-in electric field was verified by the ionic liquid of LiTFSI dissolved in DMSO. The formation of the built-in electric field from UV irradiation was not affected by the type of solvents. Remote charging of ionic current was accomplished by UV irradiation to supply charge, which could control the conversion of AC-DC signals in-situ, achieving a photo-ionic current coupling. This work not only provided a paradigm to adjust electronic displace current with ionic current but also presents a strategy for the detection of UV and other irradiation by the DC-TENGs through the conversion of signal modes. This heralds an alternative to rectify TENG for DC output, which had great potential applications in wearable devices, bioelectronics, and self-powered intelligent sensors.

4. Materials and methods

4.1. Materials

GO was synthesized by Hummers method, more details could refer to our previous work. The rGO solution was prepared by adding KOH (0.1 mol/L) into GO (5 mg/mL) solution with a 1:2 (vol/vol) ratio. The thickness of Kapton tape was 50 μm. All related reagents, including ITO electrodes, were purchased from Sigma-Aldrich, and used as received. The light source was an LED UV lamp (wavelength 365 nm) with power regulated by distance and fixed at 350 mW/cm^2 for all experiments.

4.2. Fabrication of iontronic DC-TENG

GO and rGO solutions (200 μL, respectively) were drop-casted onto ITO electrode to form the iontronic unit, forming a membrane (1 cm^2, respectively). Then, a piece of Kapton film tape (effective area of about 1 cm^2) was attached on one side of the ITO electrode to prepare TENG.

4.3. Characterization and measurements

All electrochemical properties were carried out by electrochemical workstation (Multi Auto-lab M204). Electrochemical impedance spectroscopy (EIS) was measured in the range of 0.1 MHz to 1 Hz. Electrochemical experiments related to temperature and relative humidity (RH) are performed in an environmental simulation chamber (Vötsch Technik). The surface morphologies of GO and rGO were observed by the SEM (SU8020, Hitachi) with the 5.0 kV accelerating voltage. Fourier-transform infrared (FTIR) spectra were collected by Bruker VERTEX80v. Light irradiation temperature was tested by thermal imager (UTi120S Thermal Imager). A step motor (Linear Motion 1100) was used to provide the input of mechanical motions. TENG signal data was obtained by using Keithley electrometer 6514. TENG-related experiments were conducted in a homemade humidity chamber controlled by an automatic temperature and humidity sensing system.

CRediT authorship contribution statement

D.W. and Z.L.W. proposed the idea and the project. D.W. designed all the experiments and supervised the whole project. Y.W.O.Y. carried out the experiments in this paper and analyzed the corresponding data. X.L. and S.X.L. assisted in experimental testing. P.G.P. and F.Y.Y. built the test platform. All the authors discussed the results and commented on the manuscript. D.W. and Y.W.O.Y. wrote this paper.

Declaration of Competing Interest

The authors declare no conflict of interests.

Data availability

Data will be made available on request.

Appendix A. Supporting information

Supplementary data associated with this article can be found in the online version at doi:10.1016/j.nanoen.2023.108796.

References

[1] S. Niu, X. Wang, F. Yi, Y.S. Zhou, Z.L. Wang, A universal self-charging system driven by random biomechanical energy for sustainable operation of mobile electronics, Nat. Commun. 6 (2015) 8975.
[2] X. Tang, X. Wang, R. Cattley, F. Gu, A. Ball, Energy harvesting technologies for achieving self-powered wireless sensor networks in machine condition monitoring: a review, Sensors 18 (2018) 4113.
[3] Z.L. Wang, Triboelectric nanogenerators as new energy technology and self-powered sensors – principles, problems and perspectives, Faraday Discuss. 176 (2014) 447–458.
[4] C. Wu, A.C. Wang, W. Ding, H. Guo, Z.L. Wang, Triboelectric nanogenerator: a foundation of the energy for the new era, Adv. Energy Mater. 9 (2019) 1802906.
[5] Z.L. Wang, Triboelectric nanogenerator (TENG)—sparking an energy and sensor revolution, Adv. Energy Mater. 10 (2020) 2000137.
[6] J. Chen, Z.L. Wang, Reviving vibration energy harvesting and self-powered sensing by a triboelectric nanogenerator, Joule 1 (2017) 480–521.
[7] S. Li, S. Wang, Y. Zi, Z. Wen, L. Lin, G. Zhang, Z.L. Wang, Largely improving the robustness and lifetime of triboelectric nanogenerators through automatic transition between contact and noncontact working states, ACS Nano 9 (2015) 7479–7487.
[8] Y.S. Zhou, G. Zhu, S. Niu, Y. Liu, P. Bai, Q. Jing, Z.L. Wang, Nanometer resolution self-powered static and dynamic motion sensor based on micro-grated triboelectrification, Adv. Mater. 26 (2014) 1719–1724.
[9] Q. Zhang, Q. Liang, Q. Liao, M. Ma, F. Gao, X. Zhao, Y. Song, L. Song, X. Xun, Y. Zhang, An amphiphobic hydraulic triboelectric nanogenerator for a self-cleaning and self-charging power system, Adv. Funct. Mater. 28 (2018) 1803117.
[10] J. Zhu, H. Wang, Z. Zhang, Z. Ren, Q. Shi, W. Liu, C. Lee, Continuous direct current by charge transportation for next-generation IoT and real-time virtual reality applications, Nano Energy 73 (2020), 104760.
[11] J. Wang, Z. Wu, L. Pan, R. Gao, B. Zhang, L. Yang, H. Guo, R. Liao, Z.L. Wang, Direct-current rotary-tubular triboelectric nanogenerators based on liquid-dielectrics contact for sustainable energy harvesting and chemical composition analysis, ACS Nano (2019) acsnano.8b09642.
[12] K. Zhang, X. Wang, Y. Yang, Z.L. Wang, Hybridized electromagnetic–triboelectric nanogenerator for scavenging biomechanical energy for sustainably powering wearable electronics, ACS Nano 9 (2015) 3521–3529.
[13] C. Zhang, T. Zhou, W. Tang, C. Han, L. Zhang, Z.L. Wang, Rotating-disk-based direct-current triboelectric nanogenerator, Adv. Energy Mater. 4 (2014) 1301798.
[14] J. Liu, A. Goswami, K. Jiang, F. Khan, S. Kim, R. McGee, Z. Li, Z. Hu, J. Lee, T. Thundat, Direct-current triboelectricity generation by a sliding Schottky nanocontact on MoS2 multilayers, Nat. Nanotechnol. 13 (2018) 112–116.
[15] J. Luo, L. Xu, W. Tang, T. Jiang, F.R. Fan, Y. Pang, L. Chen, Y. Zhang, Z.L. Wang, Direct-current triboelectric nanogenerator realized by air breakdown induced ionized air channel, Adv. Energy Mater. 8 (2018) 1800889.
[16] R.D.I.G. Dharmasena, H.M. Cronin, R.A. Dorey, S.R.P. Silva, Direct current contact-mode triboelectric nanogenerators via systematic phase shifting, Nano Energy 75 (2020), 104887.

[17] H. Ryu, J.H. Lee, U. Khan, S.S. Kwak, R. Hinchet, S.-W. Kim, Sustainable direct current powering a triboelectric nanogenerator via a novel asymmetrical design, Energy Environ. Sci. 11 (2018) 2057–2063.
[18] Y. Yang, H. Zhang, Z.L. Wang, Direct-current triboelectric generator, Adv. Funct. Mater. 24 (2014) 3745–3750.
[19] H. Yoon, M. Kang, W. Seung, S.S. Kwak, J. Kim, H.T. Kim, S. Kim, Microdischarge-based direct current triboelectric nanogenerator via accumulation of triboelectric charge in atmospheric condition, Adv. Energy Mater. 10 (2020) 2000730.
[20] Z. Tian, J. Li, L. Liu, H. Wu, X. Hu, M. Xie, Y. Zhu, X. Chen, W. Ou-Yang, Machine learning-assisted self-powered intelligent sensing systems based on triboelectricity, Nano Energy 113 (2023), 108559.
[21] X. Han, J. Niu, Y. Wang, X. Jin, L. Peng, J. Chen, X. Wei, X. Liu, W. Wang, H. Wang, T. Lin, Polyaniline-based Schottky-triboelectric hybrid DC generators with tunable electrical outputs, Nano Energy 104 (2022), 107956.
[22] X. Xu, J. Li, X. Tao, Q. Yan, H. Wu, Z. Guan, L. Liu, X. Chen, W. Ou-Yang, Study of interfacial design for direct-current tribovoltaic generators, Nano Energy 94 (2022), 106957.
[23] Y. Song, N. Wang, Y. Wang, R. Zhang, H. Olin, Y. Yang, Direct current triboelectric nanogenerators, Adv. Energy Mater. 10 (2020) 2002756.
[24] H. Chun, T.D. Chung, Iontronics, Annu. Rev. Anal. Chem. 8 (2015) 441–462.
[25] H. Qian, D. Wei, Z. Wang, Bionic iontronics based on nano-confined structures, Nano Res. (2023).
[26] Y. He, J. Wu, M. Lin, S. Xiao, H. Liu, P. Zhou, Ionic flexible force sensors and their potential applications, J. Mater. Chem. C 9 (2021) 16378–16390.
[27] Y. Zhou, Y. Hou, Q. Li, L. Yang, Y. Cao, K.H. Choi, Q. Wang, Q.M. Zhang, Biocompatible and flexible hydrogel diode-based mechanical energy harvesting, Adv. Mater. Technol. 2 (2017) 1700118.
[28] Y. Su, M.S. Toftdal, A. Le Friec, M. Dong, X. Han, M. Chen, 3D electrospun synthetic extracellular matrix for tissue regeneration, Small Sci. 1 (2021) 2100003.
[29] Y. Jiang, B. Tian, Inorganic semiconductor biointerfaces, Nat. Rev. Mater. 3 (2018) 473–490.
[30] C. Yang, S. Cheng, X. Yao, G. Nian, Q. Liu, Z. Suo, Ionotronic luminescent fibers, fabrics, and other configurations, Adv. Mater. 32 (2020) 2005545.
[31] R. Peng, Y. Pan, Z. Li, S. Zhang, A.R. Wheeler, X. (Shirley) Tang, X. Liu, Ionotronics based on horizontally aligned carbon nanotubes, Adv. Funct. Mater. 30 (2020) 2003177.
[32] G. Pérez-Mitta, A.G. Albesa, C. Trautmann, M.E. Toimil-Molares, O. Azzaroni, Bioinspired integrated nanosystems based on solid-state nanopores: “iontronic” transduction of biological, chemical and physical stimuli, Chem. Sci. 8 (2017) 890–913.
[33] Y. Chang, L. Wang, R. Li, Z. Zhang, Q. Wang, J. Yang, C.F. Guo, T. Pan, First decade of interfacial iontronic sensing: from droplet sensors to artificial skins, Adv. Mater. 33 (2021) 2003464.
[34] C. Yang, Z. Suo, Hydrogel ionotronics, Nat. Rev. Mater. 3 (2018) 125–142.
[35] X. Zhang, Q. Wen, L. Wang, L. Ding, J. Yang, D. Ji, Y. Zhang, L. Jiang, W. Guo, Asymmetric electrokinetic proton transport through 2D nanofluidic heterojunctions, ACS Nano 13 (2019) 4238–4245.
[36] Z. Zhang, X.-Y. Kong, K. Xiao, Q. Liu, G. Xie, P. Li, J. Ma, Y. Tian, L. Wen, L. Jiang, Engineered asymmetric heterogeneous membrane: a concentration-gradient-driven energy harvesting device, J. Am. Chem. Soc. 137 (2015) 14765–14772.
[37] Y. Huang, H. Cheng, C. Yang, P. Zhang, Q. Liao, H. Yao, G. Shi, L. Qu, Interface-mediated hygroelectric generator with an output voltage approaching 1.5 volts, Nat. Commun. 9 (2018) 4166.
[38] J. Yang, X. Hu, X. Kong, P. Jia, D. Ji, D. Quan, L. Wang, Q. Wen, D. Lu, J. Wu, L. Jiang, W. Guo, Photo-induced ultrafast active ion transport through graphene oxide membranes, Nat. Commun. 10 (2019) 1171.
[39] K. Xiao, L. Chen, R. Chen, T. Heil, S.D.C. Lemus, F. Fan, L. Wen, L. Jiang, M. Antonietti, Artificial light-driven ion pump for photoelectric energy conversion, Nat. Commun. 10 (2019) 74.
[40] D. Wei, F. Yang, Z. Jiang, Z. Wang, Flexible iontronics based on 2D nanofluidic material, Nat. Commun. 13 (2022) 4965.
[41] L. Yang, F. Yang, X. Liu, K. Li, Y. Zhou, Y. Wang, T. Yu, M. Zhong, X. Xu, L. Zhang, W. Shen, D. Wei, A moisture-enabled fully printable power source inspired by electric eels, Proc. Natl. Acad. Sci. 118 (2021) e2023164118.
[42] J. Wang, C. Wu, Y. Dai, Z. Zhao, A. Wang, T. Zhang, Z.L. Wang, Achieving ultrahigh triboelectric charge density for efficient energy harvesting, Nat. Commun. 8 (2017) 88.
[43] S. Wang, Y. Xie, S. Niu, L. Lin, C. Liu, Y.S. Zhou, Z.L. Wang, Maximum surface charge density for triboelectric nanogenerators achieved by ionized-air injection: methodology and theoretical understanding, Adv. Mater. 26 (2014) 6720–6728.
[44] D. Liu, Y. Gao, L. Zhou, J. Wang, Z.L. Wang, Recent advances in high-performance triboelectric nanogenerators, Nano Res. (2023).
[45] J. Wang, S. Li, F. Yi, Y. Zi, J. Lin, X. Wang, Y. Xu, Z.L. Wang, Sustainably powering wearable electronics solely by biomechanical energy, Nat. Commun. 7 (2016) 12744.
[46] J. Wu, Y. Xi, Y. Shi, Toward wear-resistive, highly durable and high performance triboelectric nanogenerator through interface liquid lubrication, Nano Energy 72 (2020), 104659.
[47] C. Wu, T.W. Kim, H.Y. Choi, Reduced graphene-oxide acting as electron-trapping sites in the friction layer for giant triboelectric enhancement, Nano Energy 32 (2017) 542–550.
[48] S. Xu, L. Zhang, W. Ding, H. Guo, X. Wang, Z.L. Wang, Self-doubled-rectification of triboelectric nanogenerator, Nano Energy 66 (2019), 104165.
[49] S. Li, D. Liu, Z. Zhao, L. Zhou, X. Yin, X. Li, Y. Gao, C. Zhang, Q. Zhang, J. Wang, Z. L. Wang, A fully self-powered vibration monitoring system driven by dual-mode triboelectric nanogenerators, ACS Nano 14 (2020) 2475–2482.
[50] Y. Matsumoto, M. Koinuma, S. Ida, S. Hayami, T. Taniguchi, K. Hatakeyama, H. Tateishi, Y. Watanabe, S. Amano, Photoreaction of graphene oxide nanosheets in water, J. Phys. Chem. C 115 (2011) 19280–19286.
[51] X. Qi, X. Zou, Z. Huang, L. Ren, G. Hao, Y. Liu, X. Wei, J. Zhong, Ultraviolet, visible, and near infrared photoresponse properties of solution processed graphene oxide, Appl. Surf. Sci. 266 (2013) 332–336.
[52] B. Chitara, S.B. Krupanidhi, C.N.R. Rao, Solution processed reduced graphene oxide ultraviolet detector, Appl. Phys. Lett. 99 (2011), 113114.
[53] H. Chang, Z. Sun, Q. Yuan, F. Ding, X. Tao, F. Yan, Z. Zheng, Thin film field-effect phototransistors from bandgap-tunable, solution-processed, few-layer reduced graphene oxide films, Adv. Mater. 22 (2010) 4872–4876.
[54] N. Wang, W. Zhang, Z. Li, S. Wang, A. Suwardi, E. Ye, B. Li, Y. Liu, Z. Wu, Y. Dong, X.J. Loh, D. Wang, Dual-electric-polarity augmented cyanoethyl cellulose-based triboelectric nanogenerator with ultra-high triboelectric charge density and enhanced electrical output property at high humidity, Nano Energy 103 (2022), 107748.
[55] V. Nguyen, R. Zhu, R. Yang, Environmental effects on nanogenerators, Nano Energy 14 (2015) 49–61.
[56] R. Wen, J. Guo, A. Yu, J. Zhai, Z. lin Wang, Humidity-resistive triboelectric nanogenerator fabricated using metal organic framework composite, Adv. Funct. Mater. 29 (2019) 1807655.
[57] Y. Zhang, F. Li, X. Kong, T. Xue, D. Liu, P. Jia, L. Wang, L. Ding, H. Dong, D. Lu, L. Jiang, W. Guo, Photoinduced directional proton transport through printed asymmetric graphene oxide superstructures: a new driving mechanism under full-area light illumination, Adv. Funct. Mater. 30 (2020) 1907549.
[58] L. Chen, N.S. Alharbi, C. Chen, X. Ren, UV-induced simultaneous removal of GO and U(VI): the role of aggregation, photo-transformation, adsorption and reduction, Colloids Surf. Physicochem. Eng. Asp. 648 (2022), 129151.
[59] M. Minella, M. Demontis, M. Sarro, F. Sordello, P. Calza, C. Minero, Photochemical stability and reactivity of graphene oxide, J. Mater. Sci. 50 (2015) 2399–2409.
[60] S. Cao, C. Chen, T. Liu, Y. Tsang, X. Zhang, W. Yu, W. Chen, Synthesis of reduced graphene oxide/α-Bi2Mo3O12 @ β-Bi2O3 heterojunctions by organic electrolytes assisted UV-excited method, Chem. Eng. J. 257 (2014) 309–316.
[61] T. Li, A.D. Pickel, Y. Yao, Y. Chen, Y. Zeng, S.D. Lacey, Y. Li, Y. Wang, J. Dai, Y. Wang, B. Yang, M.S. Fuhrer, A. Marconnet, C. Dames, D.H. Drew, L. Hu, Thermoelectric properties and performance of flexible reduced graphene oxide films up to 3,000 K, Nat. Energy 3 (2018) 148–156.
[62] J. Yang, X. Hu, X. Kong, P. Jia, D. Ji, D. Quan, L. Wang, Q. Wen, D. Lu, J. Wu, L. Jiang, W. Guo, Photo-induced ultrafast active ion transport through graphene oxide membranes, Nat. Commun. 10 (2019) 1171.
[63] A. Lerf, A. Buchsteiner, J. Pieper, S. Schöttl, I. Dekany, T. Szabo, H.P. Boehm, Hydration behavior and dynamics of water molecules in graphite oxide, J. Phys. Chem. Solids 67 (2006) 1106–1110.
[64] X. Qi, X. Zou, Z. Huang, L. Ren, G. Hao, Y. Liu, X. Wei, J. Zhong, Ultraviolet, visible, and near infrared photoresponse properties of solution processed graphene oxide, Appl. Surf. Sci. 266 (2013) 332–336.

Yaowen Ouyang received the B.S., M.S. degrees from the Hubei University of Technology and Sichuan University, respectively. Now, he is pursuing the Ph.D. degree at the Beijing Institute of Nanoenergy Nanosystems. His research interest is the integrated application of iontronics and TENG.

Xiang Li achieved the B.S. degree from the Shenyang University of Technology in 2018 and the M.S. degree from Shenyang Jianzhu University. Now, he continues pursuing the Ph.D. degree at Beijing Institute of Nanoenergy and Nanosystems. His research interest is solid-liquid contact electrification.

Shaoxin Li is a post-doctor in the Beijing Institute of Nanoenergy and Nanosystems. She achieved the Ph.D degree from the University of Chinese Academy of Sciences in 2022 and the B.S. degree from the Jiangsu University in 2017. Her research interest is self-powered sensors, energy harvesting, and solid-liquid contact electrification.

Puguang Peng achieved the B.S. and M.S. degrees from the Xiangtan University in 2019 and 2022, respectively. He continues pursuing Ph.D. degree in Beijing Institute of Nanoenergy and Nanosystems, Chinese Academy of Sciences. He focuses on the transformation of ions and electrons, with the applications in iontronics, energy technology and intelligent sensing systems.

Feiyao Yang is a senior engineer of Beijing Institute of Nanoenergy and Nanosystems, Chinese Academy of Sciences. He has working experience of more than ten years in the printing industry. His research interests are triboelectric nanogenerators, 2D nanofluidic materials, osmotic power source, printable electronics, and iontronics.

Prof. Zhong Lin Wang received his Ph.D. from Arizona State University in physics. He now is the Hightower Chair in Materials Science and Engineering, Regents' Professor, Engineering Distinguished Professor and Director, Center for Nanostructure Characterization, at Georgia Tech. Dr. Wang has made original and innovative contributions to the synthesis, discovery, characterization and understanding of fundamental physical properties of oxide nanobelts and nanowires, as well as applications of nanowires in energy sciences, electronics, optoelectronics and biological science. His discovery and breakthroughs in developing nanogenerators established the principle and technological road map for harvesting mechanical energy from environment and biological systems for powering personal electronics. His research on self-powered nanosystems has inspired the worldwide effort in academia and industry for studying energy for micro-nano-systems, which is now a distinct disciplinary in energy research and future sensor networks. He coined and pioneered the field of piezotronics and piezophototronics by introducing piezoelectric potential gated charge transport process in fabricating new electronic and optoelectronic devices. Details can be found at: http://www.nanoscience.gatech.edu.

Prof. Di Wei is the principle investigator at BINN, Head of the Flexible Iontronics Laboratory. As the Fellow of the Royal Society of Chemistry (FRSC) and Senior Member of Wolfson College at Cambridge University, he has published over 100 papers including Nature Energy, Nature Commun., PNAS, Adv Mater, Energy Environ Sci., Matter etc. Till end of 2022, more than 160 international patents (including PCT) have been applied, 57 international patents and 27 Chinese patents have been granted. He also edited 3 English books published in Wiley and Cambridge University Press etc. focusing on nanotechnology for energy and sensors.